The MODIS 2.1-μm Channel—Correlation with Visible Reflectance for Use in Remote Sensing of Aerosol

Yoram J. Kaufman, Andrew E. Wald, Lorraine A. Remer, Bo-Cai Gao, Rong-Rong Li, and Luke Flynn

***Abstract*—A new technique for remote sensing of aerosol over the land and for atmospheric correction of Earth imagery is developed. It is based on detection of dark surface targets in the blue and red channels, as in previous methods, but uses the 2.1-μm channel, instead of the 3.75 μm for their detection. A 2.1-μm channel is present on ADEOS OCTS and GLI, and planned on EOS-MODIS and EOSP, and a similar 2.2-μm channel is present on Landsat TM. The advantage of the 2.1-μm channel over the 3.75-μm channel is that it is not affected by emitted radiation. The 2.1-μm channel is transparent to most aerosol types (except dust) and therefore can be used to detect dark surface targets. Correlation between the surface reflection in the blue (0.49 μm), red (0.66 μm), and 2.1 μm is established using atmospherically corrected Landsat TM and AVIRIS aircraft images collected over the Eastern United States, Maine, and California and spectral data obtained from the ground and light aircraft near San Diego, CA. Results from a variety of surface covers show that the surface reflectance at 0.49 μm ($\rho_{0.49}$) and 0.66 μm ($\rho_{0.66}$) can be predicted from that at 2.2 μm ($\rho_{2.2}$) within $\Delta\rho = \pm 0.006$ for $\rho_{2.2} \leq 0.10$, using $\rho_{0.49} = \rho_{2.2}/4$ and $\rho_{0.66} = \rho_{2.2}/2$. Error in surface reflectance of 0.006 corresponds to an error in remote sensing of aerosol optical thickness, τ, of $\Delta\tau \sim \pm 0.06$. These relationships were validated using spectral data taken close to the surface over vegetated areas in a different biome. This method expands application of dark targets for remote sensing of aerosol to brighter, nonforested vegetation. The higher reflection of the surface at 2.2 μm than that of 3.75 μm may even enable remote sensing of dust above surfaces with reflectivity $\rho_{2.2} = 0.15 \pm 0.05$. For this reflectivity range the dust radiative effect at 2.2 μm is small, and the surface reflectance in the blue and red channels can be retrieved.**

***Index Terms*—Aerosols, atmosphere correction, remote sensing.**

I. Introduction

ROUTINE daily remote sensing of aerosol from satellites over the continents and oceans is envisioned to be the primary means of obtaining a global budget of aerosol, and of determining the contribution of anthropogenic emission, in order to be able to assess the aerosol radiative forcing on climate [19], [26]. Due to the short aerosol lifetime [2], and the resulting strong spatial variations in the aerosol concentration, ground-based stations cannot assess trends in the global aerosol budget. They are, though, very important in measuring the aerosol physical and optical properties [8], [17], [24], [35]. Recently there has been a resurgence of interest in aerosol radiative forcing of climate by direct reflection of sunlight to space [2], [20], [26] and by their effect on cloud microphysics and albedo [3], [11], [18], [22], [37]. Uncertainty in modeling this forcing is considered one of the largest uncertainties in climate modeling [6]. The remotely sensed aerosol information is also required for atmospheric correction of satellite images of surface cover [15], [31] Several satellite sensors, to be launched in the next several years, are designed to measure global aerosol concentration and properties using the spectral, angular or polarization properties of solar radiation reflected by the aerosol. The spectral properties are emphasized by the EOS-MODIS (Earth Observing System-Moderate Resolution Imaging Spectrograph) [21], [32] and ADEOS-OCTS and GLI (Advanced Earth Observing System-Ocean Color and Temperature Scanner and Global Imager) sensors. The angular characteristics are emphasized by EOS-MISR (Multiangle Imaging Spectroradiometer) [23] and ADEOS-POLDER (Polarization and Directionality of Earth's Reflectances) and the polarization measurements by POLDER [4] and EOS-EOSP (Earth Observing Scanning Polarimeter).

Operational remote sensing of aerosol over ocean is done with AVHRR [10], [29], but is untried for land. However, remote sensing of aerosol over the land is important because anthropogenic sources are located on land, so this is where a big part of the radiative forcing is concentrated [11], [20]. Remote sensing of aerosol over land is not done operationally because reflection of sunlight by the variable surface cover can be confused with the backscattering by the aerosol layer. The reflection of sunlight by the earth surface also influences the polarization signal measured from space, thus affecting detection of aerosol by polarization [4]. The lower the surface reflectance, the lower is the effect of uncertainty in the surface properties on remote sensing of aerosol using radiance or polarization. It is necessary, therefore, to develop methods to detect dark surface covers and to estimate their reflectance of sunlight under the aerosol layer.

Kaufman and Sendra [14] suggested using dense dark vegetation, usually green forests, as the dark targets and to detect them by using the vegetation index (composed of radiances in the red and near-infrared channels) measured at the top

Manuscript received April 22, 1996; revised October 2, 1996. This work was performed while A. E. Wald held a National Research Council-GSFC Research Associateship.

Y. J. Kaufman and A. E. Wald are with Goddard Space Flight Center, Greenbelt, MD 20771 USA (e-mail: wald@climate.gsfc.nasa.gov).

L. A. Remer and R.-R. Li are with Science Systems and Applications, Inc., Lanham, MD 20706 USA.

B.-C. Gao is with the Naval Research Laboratory, Washington, DC 20375 USA.

L. Flynn is with the Hawaii Institute of Geophysics and Planetology, University of Hawaii, Honolulu, HI 96822 USA.

Publisher Item Identifier S 0196-2892(97)05522-8.

of the atmosphere. Since the vegetation index is affected significantly by the aerosol [7] the threshold value that defines dense vegetation varies from image to image depending on the aerosol concentration. This serious restriction was alleviated by [9] and [13], who used the 3.75-μm channel to detect dense vegetation. The advantage of this long wavelength is that it is not affected by accumulation mode aerosol, e.g., sulfates and organic particles [13], though it is affected by dust [1]. The measured reflectance in this channel can be used to detect forested or dense vegetation pixels that are the darkest pixels over the land. In order to develop a universal threshold to detect forests, Kaufman and Remer [13] suggested correcting the radiance in this channel for the emission of thermal radiation using an IR channel at 11 μm. This correction is complicated by uncertainties in the surface emissivity and by atmospheric absorption in the IR [30].

The techniques for detecting dark surface pixels using the mid-IR could be improved in several aspects:

- Detect the dark pixels in a shorter mid-IR spectral channel that is not affected by emission of IR radiation, but for which the effect of aerosol will still not inhibit the detection of the dark pixels.
- Increase the range of admissible reflectances of the dark pixels, and therefore the spatial coverage of remote sensing of aerosol over the land by predicting the reflectance of the surface in the red and blue channels using the detected reflectance in the mid-IR instead of using a threshold. The red and blue channels are then used to detect the aerosol optical effect and loading.
- Develop a remote sensing technique that may be applicable also in the presence of dust.

In this paper, we use the 2.2-μm channel, present on the Landsat Thematic Mapper (TM), to show that the 2.1-μm channel planned for the MODIS, OCTS, GLI, and EOSP sensors, can be better than the 3.75 μm channel for detection of dark targets, estimating their reflectance in the blue and red channels and using them for remote sensing of aerosol. Vegetation spectra between 2.1 and 2.2 μm are flat enough so that there is little difference between using the TM 2.2-μm band and the MODIS 2.1-μm band for this application.

There are currently no models describing reflectance from vegetation-soil targets as a function of plant self-shadows and liquid water content, so the relations presented in this paper are entirely empirical. They are observed to hold for area-averaged scenes of a variety of dark, vegetated targets.

II. Surface Reflectance at 2.2 μm versus that at 0.49 and 0.66 μm

The 2.2-μm channel is in the next atmospheric window shortward of the 3.75 μm channel window. Its wavelength is already short enough that emission from the $\sim$300 K earth surface does not have a noticeable effect on the apparent surface reflectivity. It therefore will not be affected, like the 3.75-μm channel, by uncertainties in emission corrections although it will be affected by atmospheric absorption. The 2.2 μm wavelength is much larger than the size of most aerosol types (smoke, sulfates, etc.) so that these aerosols are transparent to solar radiation at 2.2 μm. Unlike emission corrections, there is much greater certainty in correcting for the effect of water vapor absorption once the amount of water vapor in the column is measured from the same satellite. To test its use for detecting dark targets and remote sensing of aerosol, we need to know to what extent the earth's surface reflectivity in the red and blue parts of the spectrum is correlated to that at 2.2 μm. There is also a need to test the residual effect of aerosol in this channel. Once the dark targets are detected and their reflectance estimated, remote sensing of aerosol can proceed using the methods outlined by [9] and [14].

We anticipate a correlation between the surface reflectivity in the blue or red spectral channels and the 2.2-μm channel for the same reasons such correlation was anticipated and measured between the red and the 3.75-μm channel [13]. Shadows, presence of vegetation, and presence of wetness in the soil, all tend to reduce the reflectivity in the mid-IR and the visible simultaneously. The reason is that while chlorophyll in vegetation absorbs solar radiation in the red and blue channels, the liquid water in vegetation absorbs in the 2.2 and 3.75 μm bands. The absorption is smaller at 2.2 than in 3.75. Wet soil, while being darker in these mid-IR channels due to the water absorption, is also darker in the visible part of the spectrum, because the difference between the refractive index of soil grains and the spaces between them is reduced when the spaces are filed up with water. This increases forward scattering, and so darkens the soil surface.

The physical basis for this aerosol detection scheme is illustrated in Fig. 1. The four images on the right side of the this figure were taken on a fairly clear day over Virginia, the images on the left during a smoke event over Alta Floresta, Brazil. The intensity scale of the blue, red, and 2.2-μm images for both sets of images are equal. The three Virginia images in the red, blue, and 2.2-μm channels, except for atmospheric reflectance in the blue and red channels, look similar to each other, illustrating the correlation in reflectance among these bands for vegetated land surfaces. Note that the intermediate 0.86-μm channel looks different. The two visible-wavelength Alta Floresta images show only aerosol scattering, but the 2.2 μm image is not affected by the aerosol, and reveals land surface. The aerosol detection scheme is based on the fact that the blue and red reflectance of the vegetated surface below the aerosol can be estimated from the 2.2 μm reflectance. The difference between the measured reflectance in the red/blue and this estimated surface reflectance is due to the aerosol.

To find the correlation between the reflectivity in the visible and 2.2 μm, we collected several AVIRIS and Landsat TM images, that have both the blue (0.49 μm), red (0.66 μm) and the 2.2-μm channels. Six images were collected during the SCAR-A experiment (Sulfates Clouds and Radiation experiment—Atlantic) with simultaneous measurements by sun/sky radiometers of the aerosol optical thickness for low aerosol loading as well as total column precipitable water. The images were corrected for the residual atmospheric effect including gaseous absorption at 2.2 μm. Rayleigh correction of satellite images was carried out using the known altitude of the targets and the 6s radiative transfer code [38]. Aerosol correction was carried out using sun/sky radiometer data (there was a

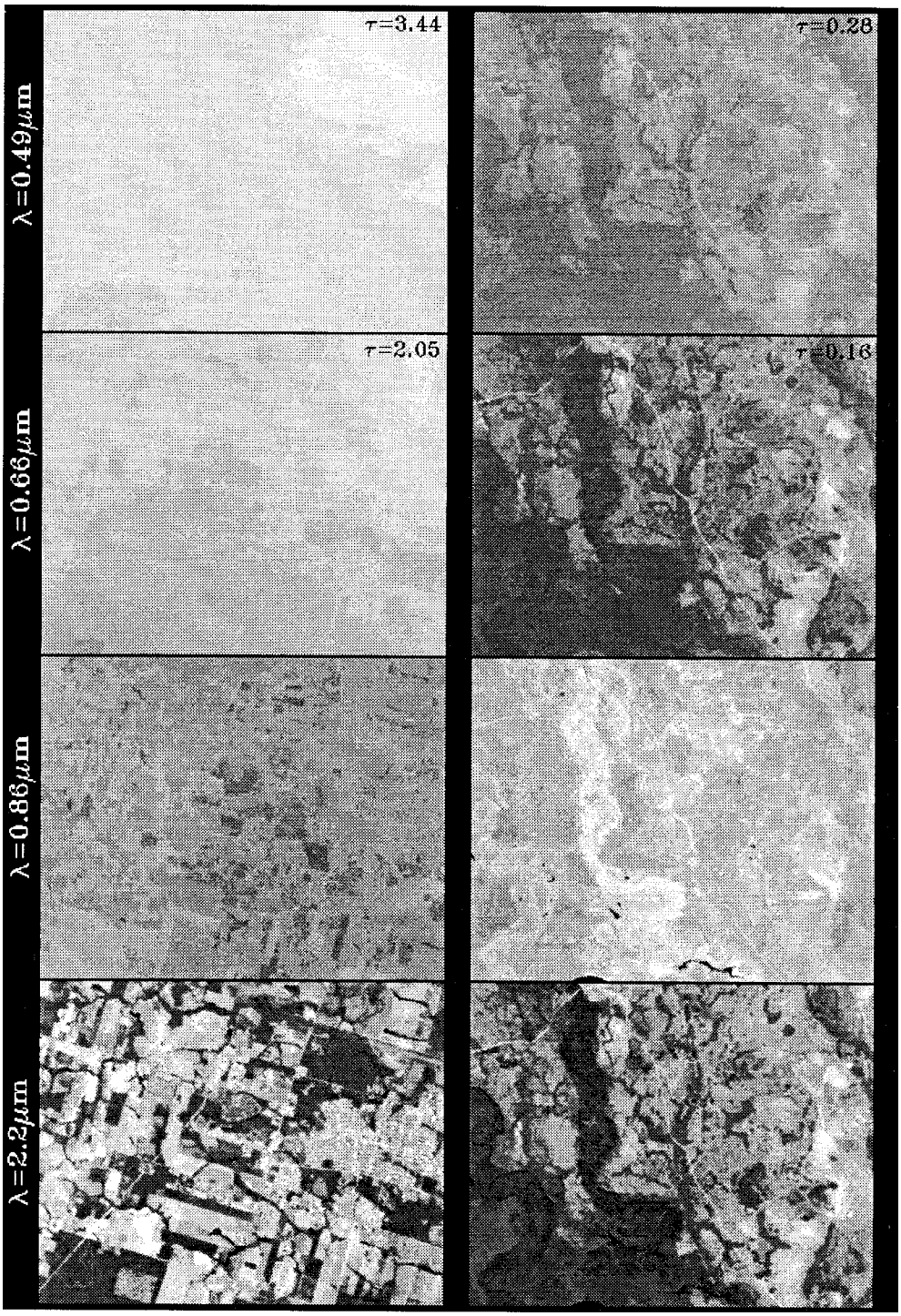

Fig. 1. Demonstration of remote sensing of aerosol using the 2.2-μm channel. The four images on the right were taken on a fairly clear day over Virginia. The four on the left were taken during a smoke event over Alta Floresta, Brazil. The spectral channel for each row of images is given in the left column. The optical depths for the visible wavelength images are also given.

radiometer located in each image) to establish aerosol optical depth, which was then used in the 6s code [38]. Typically the reflectance due to path radiance was about 0.08 in the blue, 0.03 in the red, and 0.001 at 2.1 μm. The transmission was about 0.7–0.8 for all three wavelengths. The accuracy of the atmospheric correction can be estimated by noting that Lake Drummond, VA had a post-correction reflectance of 0.004 at 2.1 μm. Water should have zero reflectance at 2.1 μm, so this residual reflectance estimates the quality of the atmospheric correction. These images, collected in July 1993 over the Eastern United States, represent green and wet surface conditions. One AVIRIS image was taken from a forested area in Howland, ME, September 1990, and one in a dry zone in Linden, CA, August 1992, to increase the range of surface cover type. For these two images the aerosol concentration was not measured but these locations are known to be low on aerosol. For each image many specific surface targets were identified and their atmospherically corrected surface spectral

TABLE I
THE LOCATION AND DATES OF THE SIX AVIRIS IMAGES AND THE TWO LANDSAT TM IMAGES USED IN THE ANALYSIS. THE SLOPE AND INTERCEPT OF THE ATMOSPHERICALLY CORRECTED REFLECTANCE AT 0.49 μm AND 0.66 μm AND THAT AT 2.2 μm ARE GIVEN AS WELL AS THE INTERCEPT FOR REFLECTANCE IN THE 2.2 μm ≤ 0.15. THE AVERAGE VALUES OF THE SLOPES (0.25 AND 0.51, RESPECTIVELY) AND THE STANDARD DEVIATIONS ARE GIVEN. THE INTERCEPT IS INTERPRETED AS A RESIDUAL AEROSOL EFFECT OR OVER CORRECTION, BUT HAS A NEGLIGIBLE EFFECT ON THE SLOPE

image information		aerosol optical thickness	slope of ρ_i vs. $\rho_{2.2}$		intercept of ρ_i vs. $\rho_{2.2}$	
Instrument, date	Location	τ_a(0.55 μm)	i=0.49 μm	i=0.66 μm	i=0.49 μm	i=0.66 μm
Landsat TM, July 12, 1993	Virginia	0.26	0.29	0.52	0.013	0.001
AVIRIS, July 12, 1993	Virginia	0.26	0.25	0.56	-0.002	-0.001
Landsat TM, July 28, 1993	Virginia	0.26	0.38	0.64	0.005	-0.01
AVIRIS, July 16, 1993	Virginia	0.24	0.20	0.50	0.006	0.001
AVIRIS, Sept. 8, 1990	Howland, Maine	<0.1	0.30	0.57	-0.009	-0.014
AVIRIS, Aug. 20, 1992	Linden, California	<0.1	0.30	0.45	0.022	0.025
AVIRIS, July 16, 1993	New Jersey	0.10	0.14	0.35	-0.004	0.005
AVIRIS, July 16, 1993 data set 1	Hagerstown, Maryland	0.10	0.13	0.50	-0.006	-0.014
AVIRIS, July 16, 1993 data set 2	Hagerstown, Maryland	0.10	0.15	0.50	-0.011	-0.014
---	---	---	---	---	---	---
average			0.26	0.51	0.005	0.002
standard deviation			0.09	0.08	0.011	0.013
average/standard deviation			3	6		

reflectance was stored. Table I summarizes the information about the images and the main results of analysis of surface spectral properties for each image.

The average slope of the relationship between the surface reflectance at 0.49 μm ($\rho_{0.49}$), 0.66 μm ($\rho_{0.66}$) and that at 2.2 μm ($\rho_{2.2}$) for the AVIRIS and TM images, given in Table I, is, respectively, three and six times larger than the standard deviation in the slope. For the average slope the reflectances $\rho_{0.49}$ and $\rho_{0.66}$, can be predicted from $\rho_{2.2}$ using

$$\rho_{0.49} = \frac{\rho_{2.2}}{4}$$

and

$$\rho_{0.66} = \frac{\rho_{2.2}}{2} \tag{1}$$

with an uncertainty, $\Delta\rho_i$, which is 1/3 and 1/6 respectively of the values of ρ_i (e.g., $\Delta\rho_{0.49}/\rho_{0.49} = \frac{1}{3}$; $\Delta\rho_{0.66}/\rho_{0.66} = \frac{1}{6}$). The intercepts between $\rho_{0.49}$, $\rho_{0.66}$, and $\rho_{2.2}$, are interpreted to be the result of residual aerosol effect or over correction of the aerosol effect. The intercepts are small, of the order of 0.005, and are much smaller for images acquired with simultaneous aerosol data than for images without such data. These errors in the atmospheric correction are mostly a bias in the red or blue radiance in each image and therefore have a negligible effect on the slopes. Note that the average value of the intercepts is much smaller than the standard deviation between them. Therefore a zero average intercept is a possible value, indicating that the intercept is likely a result of uncertainty in the atmospheric correction. To remove this atmospheric contamination, the intercepts were subtracted from the images in the analysis in this paper.

The relationship among the reflectances of the specific surface targets in these images: $\rho_{0.49}$, $\rho_{0.66}$, and $\rho_{2.2}$, are plotted in Fig. 2. A different symbol was used for each of the AVIRIS or Landsat TM images. Only data for $\rho_{2.2} \leq 0.15$ were plotted. The results indicate a correlation between the surface reflectance in the visible and mid-IR channels. The error in predicting the surface reflectance in the visible channels using the reflectance at 2.2 μm, increases with the increase in the reflectance itself. Table II summarizes the reflectances and the average absolute error in using (1) to predict the red and blue channels for several ranges of $\rho_{2.2}$. For $\rho_{2.2} \leq 0.10$, the prediction error is $\Delta\rho \sim 0.006$ for both the 0.49 and 0.66 μm channels. The error doubles for brighter surfaces ($\Delta\rho \sim 0.01$ for $0.10 \leq \rho_{2.2} \leq 0.15$). Note that the error in the derived aerosol optical thickness (τ) using the predicted value of the surface reflectance, is typically $\Delta\tau \sim 10\Delta\rho$. Therefore, for $\Delta\rho \sim 0.006$, $\Delta\tau \sim 0.06$, which

TABLE II
THE RATIO OF THE REFLECTANCE IN THE VISIBLE CHANNELS AND THE 2.2-μm CHANNEL, THE AVERAGE REFLECTANCE AT 0.49 AND 0.66 μm, AND THE AVERAGE ABSOLUTE ERROR IN PREDICTING THE REFLECTANCE USING THE REFLECTANCE AT 2.2 μm WITH (1). ERRORS LARGER THAN 0.01 ARE EMPHASIZED WITH **BOLD** LETTERS

range of $\rho_{2.2}$	$\rho_{0.49}/\rho_{2.2}$	average $\rho_{0.49}$	error in $\rho_{0.49}$	$\rho_{0.66}/\rho_{2.2}$	average $\rho_{0.66}$	error in $\rho_{0.66}$
0.0-0.05	0.25	0.011	0.006	0.52	0.023	0.005
0.05-0.1	0.19	0.014	0.007	0.47	0.033	0.007
0.1-0.15	0.27	0.033	**0.011**	0.53	0.065	**0.011**
0.15-0.25	0.20	0.039	**0.017**	0.54	0.104	**0.015**
0.25-0.40	0.25	0.071	0.008	0.62	0.173	**0.032**

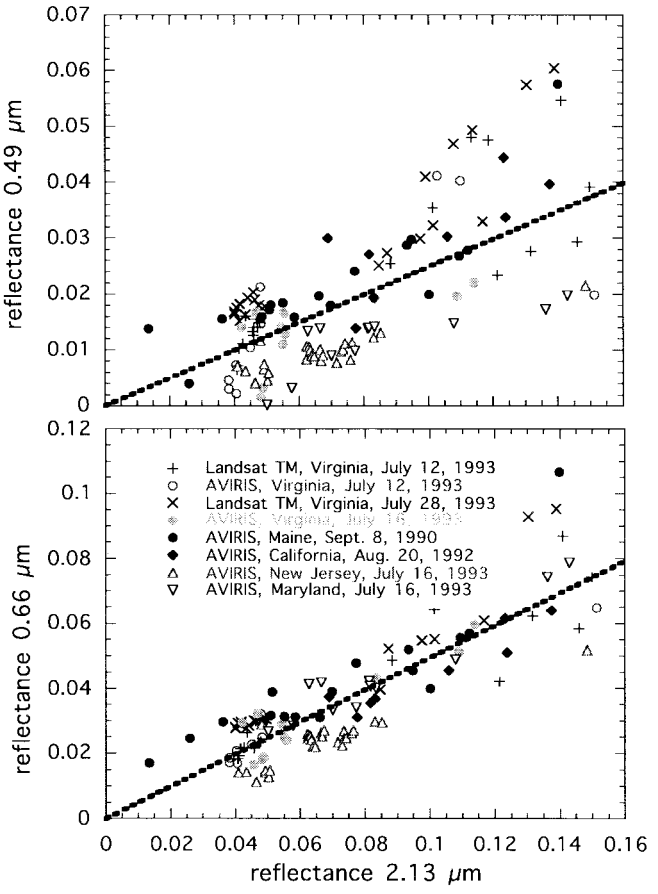

Fig. 2. Scatter diagrams between the surface reflectance at 0.49 μm ($\rho_{0.49}$), 0.66 μm ($\rho_{0.66}$), and that at 2.2 μm ($\rho_{2.2}$). A different symbol is used for each of the Landsat TM or AVIRIS images (see notations in the bottom figure). The average relationships $\rho_{0.49}/\rho_{2.2} = 0.25$ and $\rho_{0.66}/\rho_{2.2} = 0.5$ are also plotted. Only the first July 16 Maryland data set is plotted.

is a typical contribution of the uncertainty in the surface properties to the error in remote sensing of aerosol.

In order to generalize the results for global applications, the average absolute error in predicting the surface reflectance is considered separately for different surface cover types and summarized in Table III. There are four different types of forest. "Forest" represents a dense, deciduous canopy mostly found in the Virginia images. "Upland forest" is the mixed forest of the hilly terrain of western Maryland. "Pine trees" are the pine forests of the New Jersey pine barrens. "Dense vegetation" is a darker, denser land surface type interspersed within the pine forests of New Jersey. There are four categories of "natural vegetation" corresponding to the four different geographical areas: New Jersey, Virginia, Maine, and Maryland. "Natural Vegetation" represents a surface type that is green in the visible, but brighter than the forest class and visually determined not to be cultivated fields. A fifth type of natural vegetation is designated "chaparral" and represents the brushy, grayish-brown vegetation of the Sierra Nevada foothills in California. "Crop fields" represent cultivated land where rows or furrows are identified or where the land use pattern strongly suggests cultivation. "Crop field" targets span a range from a dense green canopy to mostly bare soil or stubble. "Urban area" represents residential Norfolk and includes buildings, streets and landscaping. "Soils" are very bright targets adjoining forests or natural vegetation sites in Maryland or Virginia. "Sand" refers to similar bright targets but located in New Jersey, where the soil is known to be extremely sandy.

In Table III, the surface targets from all the images used in this study, are combined for the same classes of the surface cover. The average reflectance and standard deviation are given for each channel as well as the difference between the measured (ρ_i^m) and predicted value (ρ_i^p) of the surface reflectance at $i = 0.49$ μm and $i = 0.66$ μm. The entries are organized in order of increasing reflectance at 2.2 μm. The error of prediction ($\Delta\rho_i = \rho_i^m - \rho_i^p$) varies, but it is less than or about 0.01 for a wide variety of surface covers including forests, natural vegetation, and crops. In the 0.49 μm channel the error is less than or about 0.01 for all the surface covers surveyed, except for the urban areas, even if the reflectance at 2.2 μm increases to 0.30, as for sand. The results are also plotted in Fig. 3.

III. AEROSOL SPECTRAL SIGNAL

Detection of aerosol in the blue and red channels is based on the assumption that the aerosol effect is much smaller or negligible at 2.2 μm versus that at the blue and red channels. This hypothesis is simulated for the present surface covers

TABLE III

THE AVERAGE REFLECTANCE, STANDARD DEVIATION AND, ERROR IN PREDICTING THE SURFACE REFLECTANCE AT 0.49 AND 0.66 μm FROM THAT AT 2.2 μm FOR SEVERAL CATEGORIES OF THE SURFACE COVER TYPES. THE REFLECTIVITY IN THE 2.2-μm CHANNEL. THE NUMBER OF CASES ANALYZED FOR EACH CATEGORY AND THE RATIO OF THE REFLECTANCES ARE ALSO GIVEN. ERRORS LARGER THAN 0.01 ARE EMPHASIZED WITH **BOLD** LETTERS. $\Delta\rho_i$ IS THE ERROR IN PREDICTION, ρ_i^m THE MEASURED REFLECTANCE AND ρ_i^p THE PREDICTED REFLECTANCE FOR CHANNEL i

surface cover	# of cases	average and std. of $\rho_{2.2}$	average and std. of $\rho_{0.49}$	average and std of $\rho_{0.66}$
forest	33	0.045±0.04	0.012±0.02	0.024±0.03
dense vegetation	7	0.047±0.04	0.006±0.02	0.014±0.03
upland forest	33	0.069±0.05	0.011±0.01	0.035±0.02
pine trees	16	0.070±0.05	0.011±0.02	0.027±0.02
natural vegetation - NJ	5	0.083±0.05	0.013±0.02	0.032±0.03
natural vegetation - VA	7	0.089±0.05	0.028±0.02	0.053±0.03
chapperal	9	0.113±0.04	0.035±0.02	0.056±0.03
natural vegetation - ME	4	0.116±0.06	0.029±0.02	0.055±0.03
urban area	11	0.129±0.05	0.054±0.01	0.090±0.02
crop fields	38	0.163±0.04	0.031±0.02	0.081±0.03
natural vegetation - MD	38	0.204±0.05	0.039±0.02	0.111±0.03
soils	15	0.257±0.06	0.067±0.01	0.171±0.02
sand	13	0.303±0.06	0.087±0.01	0.189±0.02
average		0.130	0.033	0.072

surface cover	$\Delta\rho_i=(\rho_i^m-\rho_i^p)$ for 0.49 μm	$\Delta\rho_i=(\rho_i^m-\rho_i^p)$ for 0.66 μm	$\rho_{0.49}/\rho_{2.13}$	$\rho_{0.66}/\rho_{2.13}$
forest	-0.001	0.000	0.27±0.07	0.54±0.07
dense vegetation	0.006	**0.011**	0.13±0.07	0.29±0.07
upland forest	0.007	0.001	0.17±0.05	0.52±0.06
pine trees	0.007	**0.011**	0.15±0.06	0.38±0.05
natural vegetation - NJ	0.009	**0.012**	0.16±0.07	0.41±0.08
natural vegetation - VA	-0.004	-0.005	0.32±0.05	0.61±0.08
chapperal	-0.006	0.004	0.31±0.08	0.48±0.08
natural vegetation - ME	0.001	0.007	0.26±0.07	0.48±0.09
urban area	**-0.021**	**-0.021**	0.42±0.06	0.69±0.07
crop fields	**0.011**	0.005	0.20±0.06	0.50±0.07
natural vegetation - MD	**0.011**	0.005	0.19±0.09	0.53±0.08
soils	-0.000	**-0.035**	0.26±0.05	0.65±0.06
sand	-0.008	**-0.028**	0.29±0.05	0.64±0.06
average	-0.001	-0.007	0.24	0.52

TABLE IV
THE EFFECT OF AEROSOL FOR CONTINENTAL AND BACKGROUND DUST MODELS ON THE OBSERVED REFLECTANCE FROM SPACE AT 0.49, 0.66, AND 2.2 μm. THE AEROSOL OPTICAL DEPTH USED IN THE MODEL WAS 0.25 AT 0.55 μm. THE SHADED AREA INDICATES SURFACE COVERS FOR WHICH THE EFFECT OF DUST AEROSOL ON THE 2.2-μm CHANNEL IS SMALL: $\Delta\rho^*_{2.2} \leq 0.01$, WHERE $\rho*$ IS THE APPARENT REFLECTANCE AT THE TOP OF ATMOSPHERE

surface cover	surface reflect. ρ	ρ*(cont. aerosol)-ρ*(no aerosol)			ρ*(dust aerosol)-ρ*(no aerosol)		
	2.2 μm	0.49 μm	0.66 μm	2.2 μm	0.49 μm	0.66 μm	2.2 μm
forest	0.045	0.033	0.021	0.001	0.029	0.027	0.013
dense vegetation	0.047	0.034	0.023	0.001	0.030	0.029	0.013
upland forest	0.069	0.033	0.019	0.000	0.029	0.026	0.010
pine trees	0.070	0.033	0.020	0.000	0.029	0.027	0.010
natural vegetation - NJ	0.083	0.032	0.020	-0.001	0.029	0.026	0.009
natural vegetation - VA	0.089	0.029	0.016	-0.001	0.026	0.023	0.008
chapperal	0.113	0.027	0.016	-0.002	0.025	0.023	0.006
natural vegetation - ME	0.116	0.029	0.016	-0.002	0.026	0.023	0.005
urban area	0.129	0.024	0.010	-0.003	0.022	0.018	0.004
crop fields	0.163	0.028	0.011	-0.004	0.026	0.019	0.001
natural vegetation - MD	0.204	0.026	0.007	-0.006	0.025	0.015	-0.003
soils	0.257	0.021	-0.003	-0.008	0.020	0.007	-0.007
sand	0.303	0.016	-0.005	-0.010	0.017	0.005	-0.011

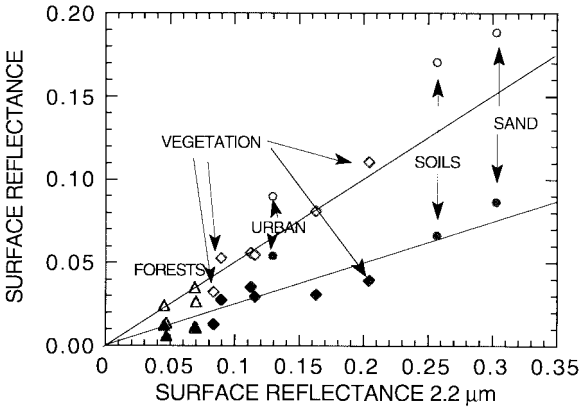

Fig. 3. Scatter diagram between the surface reflectance at 0.49 μm (full symbols) and 0.66 μm (empty symbols) to that at 2.2 μm, based on their reflectance tabulated in Table III. Several of the surface types are identified. The average relationships $\rho_{0.47}/\rho_{2.2} = \frac{1}{4}$ and $\rho_{0.66}/\rho_{2.2} = \frac{1}{2}$ are also plotted (solid lines).

using the 6S code [38] for continental and background dust models (Table IV). We define the aerosol effect as

$$\Delta\rho^* = \rho^*(\text{aerosol}) - \rho^*(\text{no aerosol}) \tag{2}$$

where ρ^* is the apparent reflectance at the top of the atmosphere. For the continental model, even for the heavy aerosol loading (optical thickness of 0.5 at 0.55 μm) the aerosol effect, $\Delta\rho^*$, on the reflectance observed from space at 2.2 μm, $\rho^*_{2.2}$, is very small. It is close to zero for forests and most other vegetation types ($\Delta\rho^*_{2.2} \leq -0.002$) increasing to $\Delta\rho^*_{2.2} = -0.01$ for soils and sand (see Fig. 4). At the same time the effect on the blue and red channels is $\Delta\rho^*_{0.49} \sim 0.03$ and $\Delta\rho^*_{0.66} \sim 0.02$. The optical effect in the blue and red channels is smaller for brighter surfaces (soils) than for darker surfaces (forests) and therefore aerosol detection is more accurate for the darker surfaces. A detailed discussion of the dependence of the aerosol effect on the surface reflectance and the aerosol properties (e.g., the single scattering albedo and the scattering phase function) was given by [5]. Continental aerosol includes large concentrations of small sulfate particles that cause the strong spectral dependence. Similar characteristics are expected from smoke particles that are as small or even smaller [16], [28].

Maritime and dust particles are much larger with a smaller spectral dependence [33], [34], [36]. Their effect on the apparent reflectance in the visible and mid IR channels is also simulated with the 6S code and shown in Fig. 3 and Table IV. While the effect of continental aerosol decreases by an order of magnitude from the visible to mid-IR, the effect of the background dust decreases only by a factor of 2. Therefore, we could expect that the present technique for remote sensing of aerosol would not work for dust.

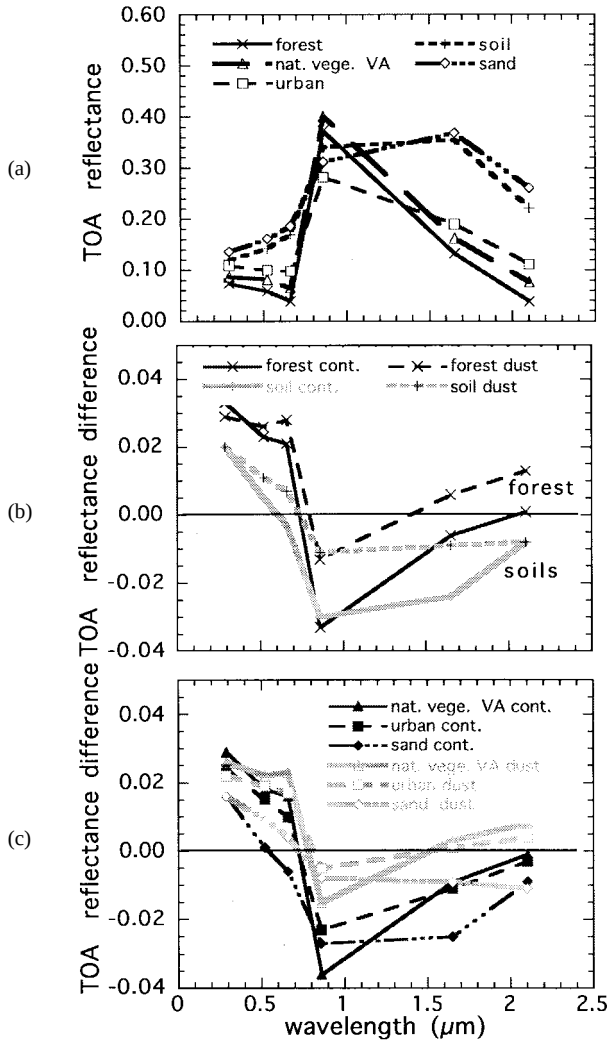

Fig. 4. (a) Top of atmosphere reflectance for forest, natural vegetation, urban areas, soil, and sand for atmosphere with no aerosol, (b) the difference between the satellite measured reflectance with and without aerosol for forest and soil, for continental aerosol and background dust for optical thickness of 0.5, and (c) same for urban area, natural vegetation, and sand.

However, the higher surface reflectance at 2.2 μm provides some help. For $\rho_{2.2} \sim 0.15 \pm 0.05$ the dust radiative effect in the present model is small ($\Delta\rho^*_{2.2} \leq 0.05$, see Table IV), because the effects of absorption and back-scattering balance out. Reflectance of $\rho_{2.2} \sim 0.15$ can be found for crops, bright natural vegetation, urban areas, and some soils. Forests are much darker ($\rho_{2.2} \sim 0.05$) and sand much brighter ($\rho_{2.2} \sim 0.30$), thus the radiative effect of dust aerosol on apparent reflectance does not cancel. The reflectance of $\rho_{2.2} \sim 0.15 \pm 0.05$, may be typical of some of the dark surfaces in semi-desert areas that are affected by dust. Pinker and Karnieli [27] conducted spectral measurements in the Israeli desert transition zone. They measured surface reflectance of less than 0.04–0.05 in the blue channel for Loessial plains, Wadi beds, some rocky terrain and sparse vegetation areas which imply that surfaces with $\rho_{2.2} \sim 0.15$ can be expected in this type of geography. For such dark surfaces, the presence of dust and its optical thickness and loading may be detected. Further studies based on spectral measurements of the surface reflectance in the semi-desert areas are needed to established the applicability of the technique to dust.

IV. Validation Using an Independent Data Set

Relationships were derived for a variety of vegetated surface types (1), with emphasis on green, wet, temperate vegetation. These relations must be validated for a variety of vegetated surface type in order to be useful for global remote sensing of aerosol. The satellite and AVIRIS images used in this study were corrected for atmospheric effects, leaving a residual error. It is therefore desirable to obtain spectral data without need for extensive atmospheric correction. To this end, we obtained visible/near-infrared spectra of semi-arid vegetation from low-flying light aircraft and from the ground near San Diego, CA, on Dec. 18–21, 1995. This type of vegetation, composed mostly of dry, olive-green scrub, is substantially different than the green, wet vegetation in most of the Landsat and AVIRIS images used in deriving (1). Spectra of these vegetated surfaces were taken by two Analytic Spectral Devices FieldSpec spectroradiometers, one owned by Goddard Space Flight Center, one by the University of Hawaii. Measurements were made at ground level in Torrey Pines State Park near the Pacific coast, and from low-flying light aircraft over surrounding areas. Targets included vegetation typical of semi-arid regions such as mixed chaparral, pine, toyon, broom, and yucca. The measurements from aircraft included similar semi-arid vegetation, plus "golden"-brown grass, cultivated land, and orchards. Spectra are averaged over the band passes of MODIS band 1 (red, 0.620–0.670 μm), band 3 (blue, 0.459–0.479 μm) and band 7 (2.2, 2.105–2.155 μm) assuming square transmission.

The data from the light aircraft were collected at altitudes of about 350 m (Fig. 7) on a day with excellent visibility and assumed minimal aerosol optical thickness. Rayleigh scattered light from the atmosphere below the airplane will contribute to the detected signal in the blue band. For ground targets with zero reflectance in the blue, the radiance detected at the airplane will equal the Rayleigh scattering contribution. Rayleigh scattering below the aircraft is negligible in the red and 2.2-μm bands. Therefore, Rayleigh scattering in the blue band for the atmosphere below the aircraft was calculated using the 6s radiative transfer code [38], and the best-fit line for the blue reflectance versus 2.2-μm reflectance is constrained to this value when the 2.2-μm reflectance is zero. The best-fit line for the red reflectance versus 2.2-μm reflectance scatterplot is constrained to pass through the origin. It is observed that, for spectra of mixed targets in the San Diego area such as those obtained from aircraft, the correlation of red and blue reflectance with 2.2-μm reflectance is given by

$$\rho_{0.49} = \frac{\rho_{2.2}}{5}$$

and

$$\rho_{0.66} = \frac{\rho_{2.2}}{2.5} \tag{3}$$

with an uncertainty, $\Delta\rho_i$, which is 1/47 and 1/16, respectively, of the values of ρ_i (e.g., $\Delta\rho_{0.49}/\rho_{0.49} = \frac{1}{47}; \Delta\rho_{0.66}/\rho_{0.66} = \frac{1}{16}$) for scenes with 2.2-$\mu$m reflectance less than about 0.25.

The coefficient for the blue reflectance in (3) is within one standard deviation of the coefficient in (1). The coefficient for the red reflectance in (3) is very close to being within one standard deviation of the coefficient in (1). The correlation for these data hold to $\rho_{2.2} = 0.25$, substantially larger than the $\rho_{2.2} = 0.15$ limit found for the satellite/AVIRIS dataset.

The standard deviation of red/blue reflectance calculated from 2.2-μm reflectance derived from the San Diego spectral data is much smaller than the standard deviation calculated from the AVIRIS and TM data. This can be due to differences in the biomes and/or due to residual errors from the atmospheric correction of the TM/AVIRIS images. While most of the TM/AVIRIS dataset was taken above green, moist vegetation, one image in the AVIRIS data set was taken in California, and consisted of chaparral. For this image, blue reflectance was 30% of the 2.2-μm reflectance, and the red reflectance was 45% of the 2.2-μm reflectance. These values are as different from the relations derived above for chaparral as chaparral is from the green, wet, temperate vegetation that constitutes most of the satellite dataset. This suggests that difference in the atmospherically corrected band correlations between two different biomes is smaller than the variation of correlation within a biome, and that (1) has wide validity.

If the relationships of (3) were used instead of (1) to predict red(blue) surface reflectance, a surface with 2.2- μm reflectance of 0.1 implies a red(blue) reflectance of 0.04(0.02) instead of the 0.05(0.025) calculated by (1). The difference in reflectance (0.01 in the red, 0.005 in the blue) corresponds to an error in aerosol optical depth of 0.05–0.1. We conclude that the error involved in applying (1) to an independent data set in a different biome remains within acceptable limits, and this conclusion supports the global application of the relationships described in (1).

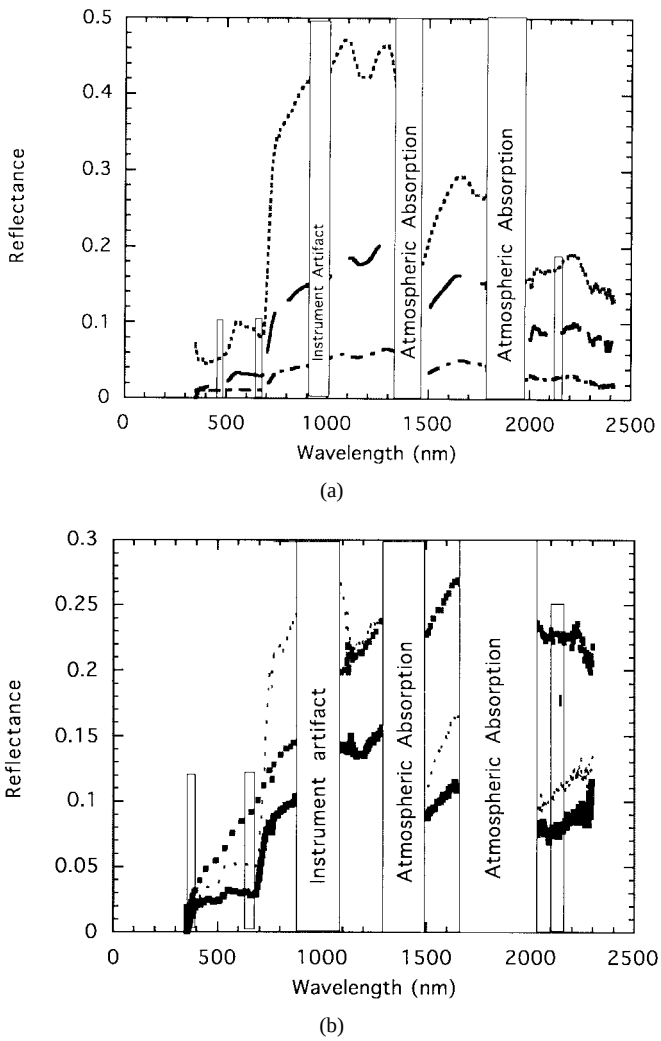

Fig. 5. (a) Sample vegetation spectra taken from ground level in Torrey Pines State Park, San Diego, CA. The targets are, from lowest to highest reflectance at 2.1 μm, sage, buckwheat, and toyon. The locations of MODIS bands 1, 3, and 7 are shown and (b) sample vegetation spectra taken from light aircraft in the same area. The targets are, from lowest to highest reflectance at 2.1 μm, dense shrub, a stand of trees, and brown grass. The locations of MODIS bands 1, 3, and 7 are shown.

V. Spatial Averaging

Fig. 5 shows some sample spectra from the ground-based measurements made in Torrey Pines State Park, and the locations of MODIS bands 1 (red), 3 (blue), and 7 (2.2 μm). Fig. 6 shows the correlation of the red and blue channels with the 2.1-μm channel for the ground-based observations. The best-fit lines for these data show that the red reflectance is one half of the 2.2-μm reflectance, but the blue reflectance is 0.34 of the 2.2-μm reflectance. However, the correlation coefficients for these fits are fairly weak. The correlation for the airborne dataset (Fig. 7) is much larger than for the ground-level measurements, a result which is due to the large-scale averaging taking place during the aircraft measurements.

The reason spatial averaging is important to achieving a strong correlation is because correlations between the visible bands and 2.1-μm band are caused by self-shadows and by liquid water-chlorophyll correlation. A typical low-resolution target composed of both illuminated leaves and shadows maps to some point on the red–2.1 μm and blue–2.1 μm plots. If this pixel is decomposed into its component shadow and light components, these individual parts also map to some point on the red–blue–2.1 μm plots. These points do not lie on the same line as the low resolution pixel because these new points do not depend on self-shadowing the same way that the large-scale pixel did. In particular, sky illumination fills in shadows in the blue but not in the red or 2.1 μm. Therefore the slope of the red–μm plot should not depend on spatial resolution (it is close to 0.5 for our ground-based, aircraft, and satellite data), but the blue–2.1 μm should (it varies between 0.25–0.34 depending on spatial resolution). Different types of plants have different proportions of shadows, causing the high-resolution data to spread about the low-resolution target line, weakening the correlation of the ground-based measurement as compared to the aircraft/satellite data.

VI. Seasonal Dependence

This aerosol detection method will only work with leafy vegetative canopies, and so depends on season. We made aircraft measurements of vegetation reflectance over Charles County, MD, on April 22 and May 22, 1996 to observe how the blue–red–2.1 μm correlation changes as a function

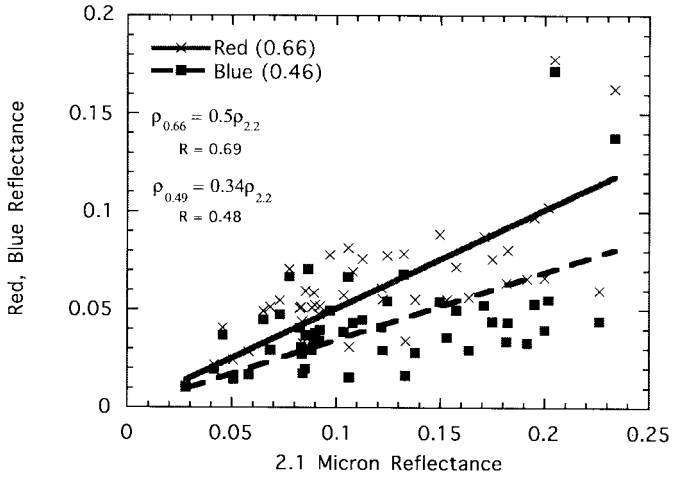

Fig. 6. Reflectance at 0.49 and 0.66 μm as a function of 2.2-μm reflectance for spectra of vegetation spectra taken at ground-level in Torrey Pines State Park, San Diego, CA.

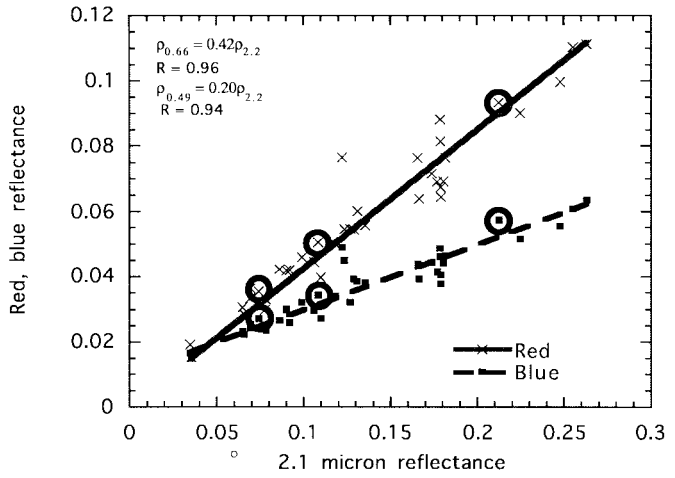

Fig. 7. Reflectance at 0.49 and 0.66 μm as a function of 2.2-μm reflectance for spectra of vegetation spectra taken from low-flying aircraft. The circled points correspond to the spectra shown in Fig. 5(b).

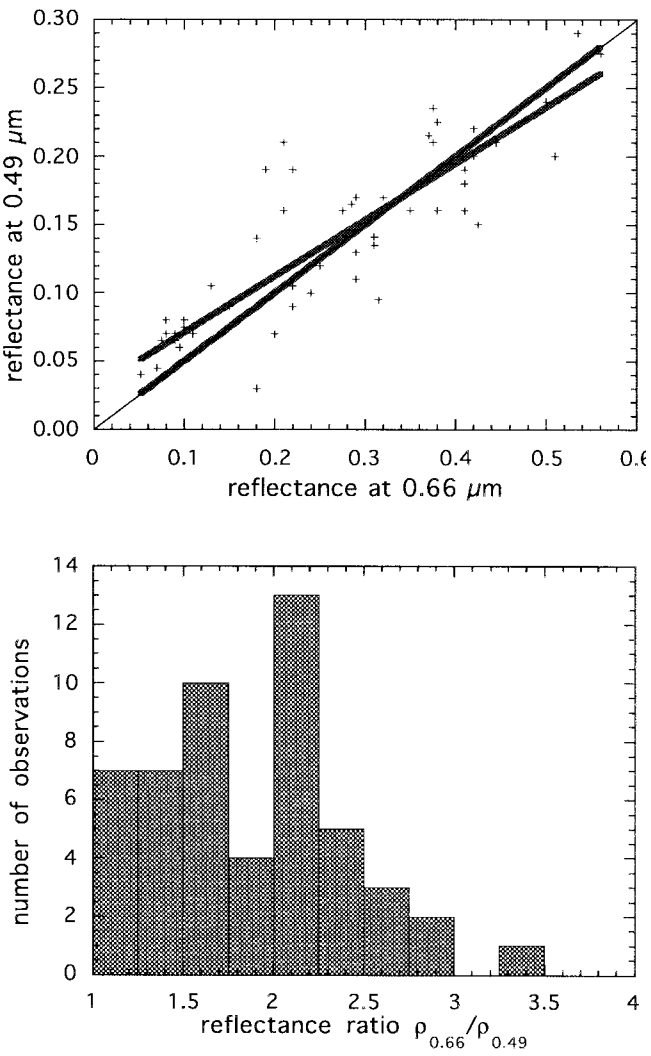

Fig. 8. Scatter diagram (top) and histogram (bottom) of the ratio between the reflectance at 0.66 and 0.49 μm computed from spectral reflectance measured in a semi-arid environment in Southern Israel [27]. The thick solid lines in the top figure are the best fits to the data assuming a linear fit and assuming a fixed ratio between the reflectances in the two channels.

of time during the growing season. On April 22, Charles County forests were starting to leaf out, but still had many bare branches. Cultivated fields were still all soil or had some small fraction of green shoots. On May 22, the forests and fields were all green. Red reflectance versus 2.1-μm reflectance for these two days is shown in Fig. 9, blue reflectance versus 2.1-μm reflectance in Fig. 10. Also plotted are best-fit lines, including Rayleigh scattering for the blue reflectance. For both April and May, there are two populations of points. The population with the largest visible reflectances and smallest 2.1-μm reflectances are those that include both vegetation and standing water in the scene. In May, the foliage has become thick enough to reduce, but not eliminate, the effect of water underneath the canopy.

Because the presence of standing water ruins the visible-near infrared correlation, it is important to determine which targets contain standing water. To do this, we plotted $\rho_{\text{blue}}/\rho_{2.1}$ versus $\rho_{0.86}$ (Fig. 10). The ratio $\rho_{\text{blue}}/\rho_{2.1}$ will be higher for spectra of vegetated targets containing standing water than for those without, and $\rho_{0.86}$ will be lower for spectra of targets containing standing water than for those without. Therefore there should be a clear separation of points on this plot corresponding to targets with standing water from points corresponding to targets without water. For both April and May, there is a threshold at about $\rho_{0.86} = 0.10$, below which are only targets containing water. These targets are all very dark (<0.05 reflectance) at 2.1 μm, and all correspond to targets that contain standing water. However, there are some spectra of targets containing standing water that do not fall below this $\rho_{0.86}$ threshold.

VII. Discussion and Conclusions

Detection of dark surface pixels as a basis for remote sensing of aerosol over the land can benefit substantially from detection of the dark pixels using the mid IR 2.2-μm band present on the Landsat TM and the 2.1-μm channel planned for the EOS-MODIS and ADEOS-OCTS, and GLI sensors. Using remote sensing data from Landsat TM and aircraft AVIRIS

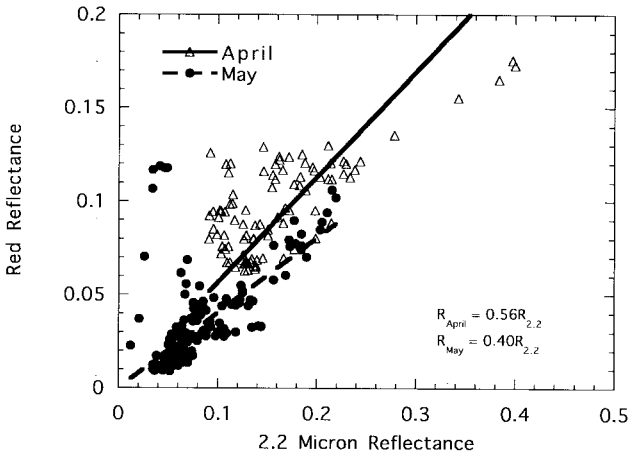

Fig. 9. Reflectance at 0.66 μm as a function of 2.2-μm reflectance for spectra of vegetation taken from low-flying aircraft over Charles County, MD, on April 22 and May 22, 1996. Also plotted are the best fit lines. The correlation between the channels gets larger and the vegetation becomes darker in both channels as the growing season progresses.

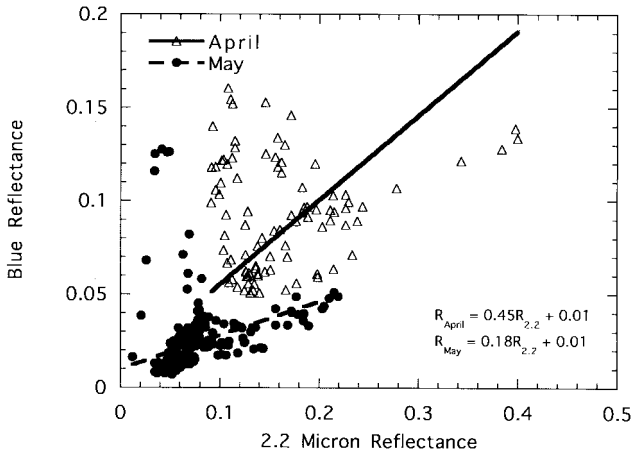

Fig. 10. Reflectance at 0.49 μm as a function of 2.2-μm reflectance for spectra of vegetation taken from low-flying aircraft over Charles County, MD, on April 22 and May 22, 1996. Also plotted are the best-fit lines, including Rayleigh scattering. The correlation between the channels gets larger and the vegetation becomes darker in both channels as the growing season progresses.

sensor, corrected for atmospheric effects including water vapor absorption at 2.2 μm, the relationships between the surface reflectance at the 0.49 μm and 0.66 μm channels and the mid-IR 2.2-μm channel were determined. Even though over 200 targets were used in the analysis, consisting primarily of green, wet temperate vegetation, but also including crops, urban areas, soils, and sand, there is a need to expand the data set for global representation. One limitation of the original data is that the TM/AVIRIS data set consisted of only nadir observations of the targets. Another is that imperfect atmospheric correction may affect the derived correlations. Differences may arise due to different transparency of leaves to the radiation and different brightness of the diffuse sky radiation.

The present results indicate that dark surface reflectance in the red (0.66 μm $-$ $\rho_{0.66}$) channel is half of that at 2.2-μm channel ($\rho_{2.2}$), and the reflectance in the blue (0.49 μm$-\rho_{0.49}$) channel is a quarter of that at 2.2-μm channel. Using this relationship, the surface reflectance in the visible channels can be predicted within $\Delta\rho_{0.49} \sim \Delta\rho_{0.66} \sim 0.006$ from $\rho_{2.2}$ for $\rho_{2.2} \leq 0.10$. This is half of the error that was obtained using the 3.75 μm [13] and corresponds to an error in the aerosol optical thickness of $\Delta\tau_a \sim 0.06$. The method was validated by ground-level and aircraft observations on semi arid vegetation that is very different than the bulk of the original satellite dataset. The independent data sets; which do not require extensive atmospheric correction, allow an extension of the calculated relationships not only to a different biome but also to nonnadir angles. Aircraft measurements were obtained at zenith angles of about 45° at a variety of azimuth angles. The results validate the original relationships in (1) for a different biome and suggest validation at nonnadir angles. Specific angles such as the direct backscattering near the vegetation "hot spot" may introduce a problem because in that direction the canopy will not be affected by self-shadowing.

We also compared (1) against 0.4–1.0 μm spectra of a semi-arid region of Israel [27]. The data can be used only to compare with the ratio of the red and blue channels. The results, shown in Fig. 8, reveal that for a wide range of surface reflectance the average ratio of the reflectance at 0.66 and 0.49 μm is 1.94, similar to the factor of 2.0 in (1). But the variability of the reflectance around the best fit line is much larger than in the data sets presented in the present paper, of the order of 0.05. These data suggest that the relationship derived in this paper hold not only in the original green, wet, temperate zone and in San Diego, but in a desert transition region as well.

The present method can be applied not only to forests but also to some brighter, lower canopies. Allowing for larger errors, remote sensing of aerosol may be expanded to grasses and crops with reflectance as high as $\rho_{0.66} = 0.08$. Other surface covers such as soil can be used to derive the optical thickness in the blue channel with an error of $\Delta\rho_{0.49} \sim 0.01$ and corresponding uncertainty in the aerosol optical thickness of $\Delta\tau_a \sim 0.1$. Previously, remote sensing of aerosol was restricted to continental and biomass burning aerosol with small particles that excluded dust [9], [13]. Using the 2.2-μm channel to detect surfaces with reflectance of $\rho_{2.2} \sim 0.15 \pm 0.05$, it is possible to detect dust as well. Dust changes the apparent reflectance in this channel for this reflectance range by only $\Delta\rho^*_{2.2} \leq 0.01$. The corresponding surface reflectances in the visible are $\rho_{0.49} = 0.020.05$ and $\rho_{0.66} = 0.050.10$, still low enough to be used to detect the dust optical thickness. Spectra taken of semi-arid vegetation suggest the possibility that this method may be extended to vegetated surfaces with $\rho_{2.2} \sim 0.25$.

Remote sensing of aerosol over the land from the MODIS sensor, planned to be launch as part of the Earth Observing System in 1998, will be based on detection of dark targets using mid-IR channels (e.g., 2.1 and 3.9 μm—[32]) and aerosol models that vary with the atmospheric conditions and are based on aerosol climatology derived from observations of the whole atmospheric column [12], [17], [25], [35]. This work is a first step in applying the 2.1-μm channel for this purpose.

REFERENCES

[1] S. A. Ackerman "Using the radiative temperature difference at 3.7 and 11 μm to track dust outbreaks," *Remote Sens. Environ.*, vol. 27, pp. 129–133, 1989.

[2] R. J. Charlson, S. E. Schwartz, J. M. Hales, R. D. Cess, J. A. Coakley, Jr., J. E. Hansen, and D. J. Hofmann, "Climate forcing by anthropogenic aerosol," *Science,* vol. 255, pp. 423–430, 1992.
[3] J. A. Coakley, Jr., R. L. Bernstein, and P. A. Durkee, "Effect of ship stack effluents on cloud reflectance," *Science,* vol. 237, pp. 953–1084, 1987.
[4] J. L. Deuzé, F. M. Bréon, P. Y. Deschamps, C. Devaux, M. Herman, A. Podaire, and J. L. Roujean, "Analysis of the POLDER (Polarization and Directionality of Earth's Reflectances) airborne instrument," *Rem. Sens. Environ.,* vol. 45, pp. 137–154, 1993.
[5] R. S. Fraser and Y. J. Kaufman, "The relative importance of scattering and absorption in remote sensing," *IEEE Trans. Geos. Rem. Sens.,* vol. 23, pp. 625–633, 1985.
[6] J. E. Hansen and A. A. Lacis, "Sun and dust versus greenhouse gases: An assessment of their relative roles in global climate change," *Nature,* vol. 346, pp. 713–719, 1990.
[7] B. N. Holben, "Characteristics of maximum value composite images for temporal AVHRR data," *Int. J. Remote Sensing,* vol. 7, pp. 1417–1437, 1986.
[8] B. N. Holben, T. F. Eck, I. Slutsker, D. Tanré, J. P. Buis, A. Setzer, E. Vermote, J. A. Reagan, Y. J. Kaufman, T. Nakajima, F. Lavenu, and I. Jankowiak, "Multi-band automatic sun and sky scanning radiometer system for measurements of aerosols," *Remote Sens. Environ.,* 1996, in press.
[9] B. N. Holben, E. Vermote, Y. J. Kaufman, D. Tanré, and V. Kalb, "Aerosols retrieval over land from AVHRR data—Application for atmospheric correction," *IEEE Trans. Geosci. Remote Sensing,* vol. 30, pp. 212–222, 1992.
[10] A. M. Ignatov, L. L. Stowe, S. Sakerin, and G. K. Korotaev, "Validation of the NOAA/NESDIS satellite aerosol product over the North Atlantic in 1989," *J. Geophys. Res.,* vol. 100, pp. 5123–5132, 1995.
[11] A. Jones, D. L. Roberts, and A. Slingo, "A climate model study of indirect radiative forcing by anthropogenic sulphate aerosols," *Nature,* vol. 370, pp. 450–453, 1994.
[12] Y. J. Kaufman, "Measurements of the aerosol optical thickness and the path radiance—Implications on aerosol remote sensing and atmospheric corrections," *J. Geophys. Res.,* vol. 98, pp. 2677–2692, 1993.
[13] Y. J. Kaufman and L. Remer, "Detection of forests using mid-IR reflectance: An application for aerosol studies," *IEEE Trans. Geosci Remote Sensing,* vol. 32, pp. 672–683, 1994.
[14] Y. J. Kaufman and C. Sendra, "Algorithm for atmospheric corrections," *Int. J. Remote Sensing,* vol. 9, pp. 1357–1381, 1988.
[15] Y. J. Kaufman and D. Tanré, "Strategy for direct and indirect methods for correcting the aerosol effect on remote sensing: From AVHRR to MODIS-EOS," *Remote Sens. Environ.,* vol. 55, pp. 65–79, 1996.
[16] Y. J. Kaufman, A. Setzer, D. Ward, D. Tanré, B. N. Holben, P. Menzel, M. C. Pereira, and R. Rasmussen, "Biomass burning airborne and spaceborne experiment in the Amazonas (BASE-A)," *J. Geophys. Res,* vol. 97, pp. 14581–14599, 1992.
[17] Y. J. Kaufman, A. Gitelson, A. Karnieli, E. Ganor, R. S. Fraser, T. Nakajima, S. Mattoo, and B. N. Holben, "Size distribution and phase function of aerosol particles retrieved from sky brightness measurements," *JGR-Atmospheres,* vol. 99, pp. 10341–10356, 1994.
[18] Y. J. Kaufman and T. Nakajima, "Effect of Amazon smoke on cloud microphysics and albedo," *J. Appl. Meteor.,* vol. 32, pp. 729–744, 1993.
[19] Y. J. Kaufman, "Remote sensing of the direct and indirect aerosol forcing," in *Aerosol Forcing of Climate,* R. J. Charlson and J. Heintzenberg, Eds. London, U.K.: Wiley, 1995, pp. 298–332.
[20] J. T. Kiehl and B. P. Briegleb, "The relative role of sulfate aerosol and greenhouse gases in climate forcing," *Science,* vol. 260, pp. 311–314, 1993.
[21] M. D. King, Y. J. Kaufman, P. Menzel, and D. Tanré, "Determination of cloud, aerosol and water vapor properties from the moderate resolution imaging spectrometer (MODIS)," *IEEE Trans. Geosci. Remote Sensing,* vol. 30, pp. 2–27, 1992.
[22] W. R. Leaitch, G. A. Isaac, J. W. Strapp, C. M. Banic, and H. A. Wiebe "The relationship between cloud droplet number concentrations and anthropogenic pollution: Observations and climatic implications," *J. Geophys. Res.,* vol. 97, pp. 2463–2474, 1992.
[23] J. V. Martonchik and D. J. Diner, "Retrieval of aerosol and land surface optical properties from multi-angle satellite imagery," *IEEE Trans. Geosci. Remote Sensing,* vol. 30, pp. 223–230, 1992.
[24] T. Nakajima, M. Tanaka, and T. Yamauchi, "Retrieval of the optical properties of aerosols from aureole and extinction data," *Appl. Opt.,* vol. 22, pp. 2951–2959, 1983.
[25] T. Nakajima, M. Tanaka, M. Yamano, M. Shiobara, K. Arao, and Y. Nakanishi, "Aerosol optical characteristics in the yellow sand events observed in May 1982 at Nagasaki—Part 2 Models," *J. Meteor. Soc. Jpn.,* vol. 67, pp. 279–291, 1989.
[26] J. E. Penner, R. E. Dickinson, and C. A. O'Neill, "Effects of aerosol from biomass burning on the global radiation budget," *Science,* vol. 256, pp. 1432–1434, 1992.
[27] R. T. Pinker and A. Karnieli, "Characteristic spectral reflectance of a semi-arid environment," *Int. J. Remote Sensing,* vol. 16, pp. 1341–1363, 1995.
[28] L. F. Radke, D. A., Hegg, P. V. Hobbs, J. D. Nance, J. H. Lyons, K. K. Laursen, P. J. Reagan, and D. E. Ward, "Particulate and trace gas emission from large biomass fires in North America," *Global Biomass Burning,* J. Levine, Ed. Cambridge, MA: MIT Press, 1991, pp. 209–224.
[29] C. R. N. Rao, E. P. McClain, and L. L. Stowe, "Remote-sensing of aerosols over the oceans using AVHRR data theory, practice and applications," *Int. J. Remote Sens.,* vol. 10, pp. 743–749, 1989.
[30] J. C. Roger and E. F. Vermote, "Computation and use of the reflectivity at 3.75 μm from AVHRR channels," in *Physical Measurements and Signature in Remote Sensing,* European Space Agency, 1994, pp. 817–824.
[31] S. W. Running, C. O. Justice, V. Salomonson, D. Hall, J. Barker, Y. J. Kaufman, A. H. Strahler, A. R. Huete, J. P. Muller, V. Vanderbilt, Z. M. Wan, P. Teillet, and D. Carneggie, "Terrestrial remote sensing science and algorithms planned for EOS/MODIS," *Int. J. Remote Sensing,* vol. 15, pp. 3587–3620, 1994.
[32] V. V. Salomonson, W. L. Barnes, P. W. Maymon, H. E. Montgomery, and H. Ostrow, "MODIS: Advanced facility instrument for studies of the earth as a system," *IEEE Trans. Geosc. Remote Sensing,* vol. 27, pp. 145–153, 1989.
[33] E. P. Shettle, "Optical and radiative properties of a desert aerosol model," *Proc. Symp. on Radiation in the Atmosphere,* G. Fiocco Ed. Fairfax, VA: A. Deepak, 1984, pp. 74–77.
[34] E. P. Shettle and R. W. Fenn, "Models for the aerosol of the lower atmosphere and the effect of humidity variations on their optical properties," Hanscom AFB, MA, Opt. Phys. Div., Air Force Geophys. Lab., 1979, AFGL-TR 790214.
[35] M. Shiobara, T. Hayasaka, T. Nakajima, and M. Tanaka, "Aerosol monitoring using a scanning spectral radiometer in Sendai, Japan," *J. Meteor. Soc. Jpn.,* vol. 69, pp. 57–70, 1991.
[36] D. Tanré, C. Devaux, M. Herman, R. Santer, and J. Y. Gac, "Radiative properties of desert aerosols by optical ground-based measurements at solar wavelengths," *J. Geophys. Res.,* vol. 83, pp. 14,223–14,231, 1988.
[37] S. A. Twomey, M. Piepgrass, and T. L. Wolfe, "An assessment of the impact of pollution on the global albedo," *Tellus,* vol. 36b, pp. 356–366, 1984.
[38] E. F. Vermote, D. Tanré, J. L. Deuze, M. Herman, and J. Morcrette, "Second simulation of the satellite signal in the solar spectrum: An overview," *IEEE Trans. Geosci. Remote Sensing,* 1996, submitted.

Yoram J. Kaufman received the B.Sc. and M.Sc. degrees in physics from the Technion—Israeli Institute of Technology, Haifa, and the Ph.D. degree from the Tel Aviv University, Yel Aviv, Israel, in 1979.

He joined NASA/Goddard Space Flight Center, Greenbelt, MD, in 1979 on an NRC fellowship award. He is currently a senior atmospheric scientist at NASA Goddard, the Project Scientist of the Earth Observing System first platform (AM1) to be launched in 1998, and a member of the EOS-MODIS science team. His present work includes theoretical and experimental research in atmospheric radiative transfer and remote sensing. It includes remote sensing of aerosol, their interaction with clouds and radiation, and impact on climate; biomass burning in the tropics; and calibration of satellite sensors. He conducted the Smoke/Sulfate, Clouds And Radiation (SCAR) field experiments in Brazil and the United States, that include measurements from aircraft and from the ground of the aerosol properties and their effect on clouds and radiation. He has about 80 refereed publications.

Dr. Kaufman received several NASA/GSFC awards, three of his papers were selected for SPIE milestone Series of outstanding papers on CO_2 lasers, and two of his papers were selected as the best paper/letter of the year by the IEEE TRANSACTIONS ON GEOSCIENCE AND REMOTE SENSING for 1992, and by the *International Journal of Remote Sensing* for 1990.

Andrew E. Wald received the B.S. degree in optics from the University of Rochester, Rochester, NY, and the M.A. degree in physics and the Ph.D. degree in earth and planetary sciences from The Johns Hopkins University, Baltimore, MD.

His work experience includes postdoctoral work in the College of Oceanic and Atmospheric Sciences, Oregon State University, Corvallis, on cloud remote sensing and also several jobs in optical engineering, including projects in lens design and testing, production of optical thin films, and adaptive optics. He is currently an NRC Research Associate in the Climate and Radiation Branch at NASA/Goddard Space Flight Center, Greenbelt, MD, working on field measurements of canopy reflectance and of forest fires, laboratory measurements of mineral reflectance, and modeling of reflectance from clouds, aerosols, vegetation, and rocks.

Lorraine A. Remer received the B.S. and Ph.D. degrees in atmospheric science from the University of California, Davis, in 1980 and 1991, respectively. She received the M.S. degree in oceanography from the Scripps Institution of Oceanography, University of California, San Diego, in 1983.

She spent three years working as a consultant providing information and assistance to the wind energy industry in California. Se is currently with Science Systems and Applications Inc., Lanham, MD, providing scientific support to the NASA EOS-MODIS science team. Her research includes modeling the optical properties of aerosols, remote sensing, atmospheric correction of satellite imagery, aerosol-cloud interaction, and aerosol effects on climate change. She lead several recent field experiments that collected data on urban/industrial aerosols over the Mid-Atlantic region of the United States and smoke aerosol in the Pacific Northwest and Brazil.

Bo-Cai Gao received the B.S. degree in physics from Nankai University, China, in 1982, and the M.S. and Ph.D. degrees in physics from The Ohio State University, Columbus, in 1984 and 1988, respectively.

He is presently with the Remote Sensing Division, Naval Research Laboratory, Washington, DC. He is conducting research in remote sensing of atmospheric water vapor, cirrus clouds and coastal water. He participated in field experiments and analysis of remote sensing data from aircraft and satellite platforms. Based on the analysis of high spatial and spectral resolution NASA/JPL Airborne Visible Infrared Imaging Spectrometer (AVIRIS) data, he discovered that the 0.94 μm water vapor band is useful for remote sensing precipitable water vapor from space over land areas and that the 1.375 μm water vapor band is very sensitive to detect thin cirrus clouds during the daytime. Both channels have been implemented on the NASA EOS/MODIS satellite instrument. He is now a member of the Earth Observing System-MODIS science team.

Dr. Gao received a Prize Paper Award for his development of an operational atmospheric radiative transfer code to retrieve surface reflectance spectra from AVIRIS data.

Rong-Rong Li received the B.S. degree in optical physics from Nankai University, China, in 1982, and the M.S. and Ph.D. degrees in physics from the University of Cincinnati, Cincinnati, OH, in 1989 and 1995, respectively.

She is currently working at the Climate and Radiation Branch of NASA/Goddard Space Flight Center, Greenbelt, MD, through the Science Systems and Applications Inc., Lanham, MD. She performed experimental studies on the thermal, electrical, and magnetic properties of commercially available ceramic chips at low temperatures. She also performed experimental studies on the dynamical properties of two-dimensional superconductor-insulator-superconductor proximity-coupled Josephson junction arrays with different amounts of defects at low temperatures. She is presently analyzing remote sensing data measured with instruments on board aircrafts and satellites, and helping the development of scientific algorithms for retrieving atmospheric aerosol information from data to be acquired with the NASA EOS-MODIS instrument.

Luke Flynn was born in Putnam, CT, on March 10, 1964. He received the B.A. degree in physics from Cornell University, Ithaca, NY, in 1986 and the Ph.D. degree in geophysics from the University of Hawaii, Honolulu, in 1992.

Since 1986, he has been working on issues related to volcanic hazard monitoring using hyperspectral field data of high-temperature eruption features. He has collected measurements and developed models demonstrating lava flow cooling. These results have been used to interpret single Landsat images showing that the short-term chronological history of the eruption and, hence, immediate hazard to surrounding areas may be rapidly assessed from satellite imagery. In 1994, he began working with Dr. Y. Kaufman and Dr. C. Justice as part of the MODIS Fire Algorithm Group. He is currently a co-investigator on the EOS Volcanology Interdisciplinary Science Team and is designing an automated thermal alert algorithm which will search the MODIS data stream in near-real time for high-temperature volcanic eruptions and fires. The alert information will be fully processed and then displayed on a web page. Updates will appear as new observations are collected. He is also a principal investigator and team member of the Hyperspectral Imager and Landsat 7 instrument teams.